JOM, Vol. 76, No. 9, 2024
https://doi.org/10.1007/s11837-024-06725-w




# Density Tuning in Conjunction with Pelletizing of Reductants for Enhanced Recovery from Copper Smelting Slag

JUN XIA,[1] HAOYU LIU,[2] HANG CHEN,[4] XIAOPENG CHI,[2,3] WEI WENG ,[2,3,5] and SHUIPING ZHONG[2,3,4,6]

1.—College of Materials Science and Engineering, Fuzhou University, Fuzhou 350108, China. 2.—Zijin School of Geology and Mining, Fuzhou University, Fuzhou 350108, China. 3.—Fujian Key Laboratory of Green Extraction and High-Value Utilization of New Energy Metals, Fuzhou University, Fuzhou 350108, China. 4.—Zijin Mining Group Co., Ltd., Shanghang, Longyan 364200, China. 5.—e-mail: wengwei198912@163.com. 6.—e-mail: zspcsu@163.com

High-efficiency reduction of $Fe_3O_4$ particles in molten copper slag is the key for recovering slag-entrained copper, although restrained by the sluggish reaction kinetics of commercial powdery reductants with low density. Here, a new strategy by density tuning in conjunction with pelletizing of the powdery reductants is suggested, greatly enhancing the $Fe_3O_4$ reduction kinetics and resulting in remarkably facilitating the recovery of slag-entrained copper. Specifically, by replacing the industrially used coal powder with $FeS_2$-C pellets at optimized density, the efficiency of $Fe_3O_4$ reduction is significantly increased from 18% to 51%, with the copper content in the low-layer slag being correspondingly enriched from 1.37% to 4.53%. The SEM-EDS characterizations and finite element analytical results all reveal that the enhanced reduction of $Fe_3O_4$ by the as-designed reductant contributes to the decrease of slag viscosity and copper exposure, as well as to the size growth of copper matte droplets, resulting in promoted settling of copper-containing components for copper–slag separation in the molten state. Additionally, the full exposure and size growth of copper matte in the molten state facilitate copper reclamation during the subsequent grinding–flotation process of the solidified slag, which increases the copper recovery from 23.3% to 85.3%, with the concentrate grade being correspondingly improved from 2.8% to 6.45% after one-stage flotation. The results can provide new insights into enhancing the recovery of slag-entrained copper.

## INTRODUCTION

Copper is one of the critical metals and the indispensable resource for society development due to its versatile applications in both traditional and newly emerging fields.[1] However, the uneven geological distribution of copper largely weakens the self-support ability for many countries.[2] For example, China only accounts for approximately 3% of the worldwide copper resource but consumes about 50% of the worldwide copper productivity, presenting a huge supply–demand gap. Thus, deep reclamation of copper during the metallurgical process is of prime importance and an effective way to mitigate the geographical restriction in the copper resource.[3,4]

Reclamation of copper from copper smelting slag has long been the strategy to improve the recovery ratio for copper smelters; however, it is hindered by the precipitated $Fe_3O_4$ particles in the molten slag.[5,6] Firstly, the entrained copper in the slag is high, up to 0.6–1.4%, greatly exceeding the mining grade of copper ore (0.4–0.8%).[7] Additionally, the generated slag amount is very large, namely the generation of 1 ton copper metal results in 2.2–3.0 tons of slag,[3,4] which means 800,000 tons of copper are entrained within the slag worldwide. Such a huge amount of copper can be hopefully recovered

(Received November 9, 2023; accepted June 17, 2024; published online July 11, 2024)

by a combination of the hot-stage process (settling of copper matte droplets for initially gross copper–slag separation in the molten state) and the subsequent cold-state step (grinding–flotation process of the solidified slag to further enrich the remaining copper).[4,8–10] However, copper recovery in both the hot-stage process and the cold-state step is hindered by the precipitated $Fe_3O_4$ particles in the molten slag.[11,12] Specifically, the precipitated $Fe_3O_4$ particles increase the viscosity of the molten slag, restraining the settling of copper matte droplets for copper–slag separation in the hot-stage process.[13,14] As for the cold-state step, the $Fe_3O_4$ phase (melting point is higher than 1500°C) is solidified preferentially and tends to wrap the copper matte droplets (the melting point is 995–1095°C).[15] However, the precipitated $Fe_3O_4$ particles are too hard to grind [which is a pre-treatment for recovering copper from copper slag (CS) by flotation] to expose the copper matte, leading to lower copper recovery.[9] High-efficiency elimination of the precipitated $Fe_3O_4$ in the molten slag is an appealing but tough task for copper recovery.

The reduction of $Fe_3O_4$ in molten slag has been the consensus for mitigating its adverse effect for copper recovery. Coal and pyrite ($FeS_2$) are the commonly used reductants for $Fe_3O_4$ elimination,[16] but suffer from very limited reaction efficiency. The low-density coal usually floats on the upper surface of the molten slag,[17,18] incapable of high-efficiency removal of the $Fe_3O_4$ particles. On the other hand, the reduction ability of $FeS_2$ is weaker than coal. Specifically, the solid $Fe_3O_4$ particles in molten CS can be easily reduced by coal at the slag temperature of 1200–1250°C ($Fe_3O_4 + C = 3FeO + CO, \Delta G^{\theta}_{1200-1250°C} < 0$). However, reduction of $Fe_3O_4$ by the FeS (generated due to spontaneous decomposition of $FeS_2$) can only occur when the temperature is higher than 1514°C ($3Fe_3O_4 + FeS = 10FeO + SO_2$, $\Delta G^{\theta} < 0$ when $T > 1514°C$). Of note, the existence of $SiO_2$ can reduce the reduction temperature of $Fe_3O_4$ from 1514°C to 1099°C ($3Fe_3O_4 + FeS + 5SiO_2 = 5Fe_2SiO_4 + SO_2, \Delta G^{\theta} < 0$ when $T > 1099°C$), promoting the reduction of $Fe_3O_4$.[19] More importantly, both coal and $FeS_2$ exist in the powdery state, which is easily blown away by the high-pressure off-gas, presenting very limited reaction efficiency. To improve the reduction efficiency, many external fields, such as the magnetic field,[20,21] mechanical field,[19,22,23] and super-gravity field,[24] have been adopted to enhance the reaction kinetics.[25–27] Nonetheless, additional equipment with high complexity is needed, so that most of the equipment is self-designed and specially made. For example, Kalisch et al.[28] developed the first industrial copper slag-cleaning furnace by an externally applied magnetic field (electromagnet) based on magnetohydrodynamics. Wang et al.[19] added a mechanical stirring system (Zhongjie, Z3050 × 16/1; Shenyang, China) to a medium-frequency induction furnace. Wang et al.[24] used a high-temperature centrifugal apparatus to simulate a super-gravity field and produced an enhanced force field in the horizontal direction. In detail, the apparatus was equipped with a heating furnace and a counterweight, and symmetrically fixed onto the centrifugal axis and rotated to the horizontal from the vertical direction once driven by the variable speed motor. Then, when it rotated at high speed, the molten slag in the furnace would be added to a super-gravity field for enhancing slag–matte separation. Moreover, integration of these new techniques with the industrial process is very difficult. Recently, a novel strategy which directly injects the powdery carbonaceous solids or waste oil into the molten slag was reported,[29–32] which can avoid the flotation of low-density reductants or the blowing away of powdery reductants by the high-pressure off-gas. Such a new injection strategy presents fascinating reaction kinetics,[29,30,33–36] which can reduce the copper content from 1.2% to 0.46% by injecting coal and pyrite into the melting slag.[37] However, the pipes used for the injection strategy are easily corroded by the high-temperature slag which has a strong oxidative ability. Also, the powdery particles with substantially reduced size for injection increase the operation risks. Exploring other strategies for improving the reaction efficiency of low-density reductants and restraining the blowing away of powdery reductants are still highly attractive.

Here, a density tuning in conjunction with a pelletizing strategy is proposed for improving the reaction kinetics of low-density and powdery reductants. Specifically, the density of the reductant is adjusted by mixing the light anthracite (C, 1.4–1.8 g/cm$^3$) with the heavy pyrite ($FeS_2$, 4.8–5.0 g/cm$^3$) to prevent the light reductant floating on the upper surface of the molten slag (3.65–3.8 g/cm$^3$). Correspondingly, the blowing away of the powdery reductants by the high-pressure off-gas can be hindered after pelletizing. In other words, the reductant in the pelletized state can restrain the blowing away by the off-gas. In addition, the reductant pellets with well-tuned density can more easily sink into the molten slag. As a result, the reductant can contact and reduce the $Fe_3O_4$ particles more smoothly to enhance the reduction kinetics in the molten slag, facilitating much enhanced slag–matte separation in the molten state and also the subsequent grinding–flotation recovery of copper in the solidified cold slag. Such a strategy is simple and free of complex equipment as well as allowing easy integration with the industrial process, providing new insights into copper recovery from the slag.

## EXPERIMENTAL

### Materials

The CS sample and matte for the experiments was provided by the copper smelting plant in Zijin Copper, with the chemical composition shown in

Table I. As revealed from the XRD patterns (Fig. 1), the copper slag mainly consists of fayalite, magnetite, and a little matte, while the copper matte mainly consists of $Cu_{1.96}S$, $CuS_2$, and $Cu_5FeS_4$.

The pyrite ($FeS_2$) was provided by Zijin Mining (– 0.15 mm in size), and the anthracite of industrial grade was from Henan Bokes. The industrial analysis of the pyrite and anthracite is shown in Table II. Sodium metasilicate pentahydrate of industrial grade was obtained from Guangzhou Zhanen Chemical. High-purity argon gas with a purity of higher than 99.999% was from Fuzhou Huaxinda Industrial Gas, which provided a protective atmosphere in the reaction. A corundum stick (diameter: 20 mm, height: 100 mm) was provided by Jingwei Special Ceramics.

## Experimental Details

Dilution experiment. This can be divided into three steps of total experiment. Firstly, for the pre-melting of the slag, 400 g dry slag powder contained in a corundum crucible (Φ70 mm × 120 mm) were put into a high-temperature furnace with a protective atmosphere by using argon gas at a flow rate of 200 mL/min. The pre-melting process of the slag sample involved heating from room temperature (about 20°C) to 1000°C at a speed of 10°C/min, then to 1250°C at 5°C/min and held at a constant temperature for 10 min. The total pre-melting time was about 158 min. A schematic of equipment is shown in Fig. 2a. Secondly, for the preparation of the reductant pellets, the anthracite powder was mixed with the $FeS_2$ powder at a fixed weight ratio, with 5 wt.% $Na_2SiO_3$ (the ratio indicates the proportion of the weight of $Na_2SiO_3$ to the total weight of $FeS_2$ and C) and a certain amount of water added as a binder for die-pressing at 20 MPa. The resultant pellets (diameter: 20 mm; height: 5 mm) have been denoted as $FeS_2$-C, which the underwent air-drying under natural conditions for 24 h, as shown in Fig. 2b. The amount of the reductant was fixed at 1% of the slag mass (that is 4 g per pellet). Therefore, only 0.05 wt.% $Na_2SiO_3$ was introduced into the slag from the pellets, meaning that the influence of the introduced $Na_2SiO_3$ for the slag composition and the refractory materials is negligible. Thirdly, for the reduction reaction, the reductant pellet was dropped into the molten slag from a height of 1 m, and the reaction time of 60 min is referred to as the staying period of the molten slag in the industrial production furnace. The contents of $FeS_2$ in the $FeS_2$-C pellets were 0, 60%, 70%, 80%, 90%, and 100%. After the reducing reaction, the slag was cooled to room temperature and sliced into three layers for analysis, as shown in Fig. 2c.

Settling experiment. For simulation of the settling behavior of the $FeS_2$-C reductant in the molten slag, a corundum pellet (diameter: 20 mm, height: 5 mm) was selected as a reaction-inert pellet, which possessed a similar density as the $FeS_2$-C reductant. The main operating steps were the same as for the reduction experiment. After standing for predetermined periods, the solidified slag was sliced to determine the final position of the reaction-inert corundum pellet.

Settling simulation of the reductant pellet and matte particle. The reductant and matte particles settling in the melting slag with different viscosities were simulated by finite element analysis. The

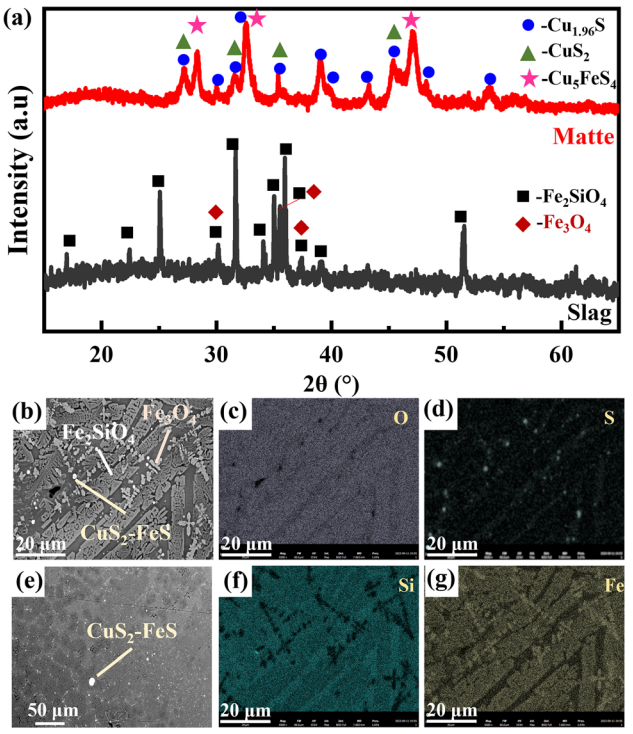


Fig. 1. (a) XRD pattern and (b, e) SEM-EDS of the copper slag and matte, (c, d, f, g) element analysis of O, S, Si, Fe, of (b).

**Table I. Chemical composition of the CS and matte (wt.%)**

| Component | Cu | S | TFe | $SiO_2$ | CaO | MgO | Pb | Zn | $Fe_3O_4$ |
|---|---|---|---|---|---|---|---|---|---|
| Slag | 1.10 | 0.84 | 39.1 | 32.14 | 2.13 | 1.33 | 0.59 | 3.38 | 18.80 |
| Matte | 61.90 | 21.15 | 11.93 | – | – | – | 1.11 | 1.24 | 2.72 |

*TFe* Total content of Fe.

**Table II. Industrial analysis of the anthracite and $FeS_2$**

| | Component | $FC_d$ | $V_d$ | $A_d$ | Total sulfur |
|---|---|---|---|---|---|
| Anthracite | Content (%) | 85.59 | 37.6 | 8.98 | 0.3 |

| | Component | $FeS_2$ | $SiO_2$ | $2Fe(OH)SO_4$ | Others |
|---|---|---|---|---|---|
| Pyrite | Content (%) | 91.20 | 3.98 | 2.08 | 2.74 |

$FC_d$, Fixed carbon; $V_d$, Volatile matter; $A_d$, Ash.

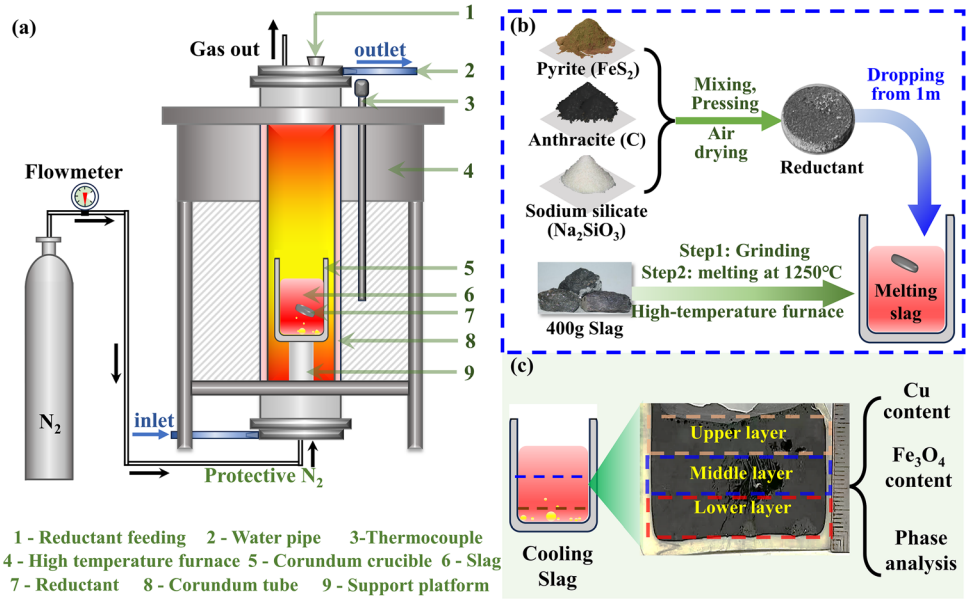


Fig. 2. Schematic of the CS dilution experiment: (a) equipment; (b) preparation of reductant and pre-treatments; (c) characterization.

viscosity of the slag ($\mu_{CS}$) was greatly affected by the content of solid particles,[12] which can be determined by:

$$\eta_r = (1 - \alpha\Phi_s)^{-n} \quad (1)$$

where $\eta_r$ is the viscosity of the slag-containing solid phase (Pa s), $\Phi_s$ is the volume fraction of the solid phase in the molten slag (%), the value of $\alpha$ is 2, and the value of $n$ is 3.95, which are the empirical parameters from reference.[12]

The velocity of matte particles in the molten slag was calculated by Stokes equations for particle settling, with the assumption of the particles being spherical with no distortion during freely falling:

$$v = \frac{gd^2(\rho_{matte} - \rho_{CS})}{18\mu} \quad (2)$$

where $v$ is the velocity of the matte particle (m/s), $d$ is the diameter of the matte particle (m), $\rho_{matte}$ is the density of matte (5200 kg/m$^3$), $\rho_{CS}$ is the density of CS (3700 kg/m$^3$), and $\mu$ is the viscosity of melting CS (Pa s).

The reduction efficiency of the $Fe_3O_4$ was calculated by:

$$E_r = \frac{m_{rb} - m_{ra}}{m_{rb}} \times 100\% \quad (3)$$

where $E_r$ is the reduction efficiency of $Fe_3O_4$ (%), $m_{rb}$ is the mass of $Fe_3O_4$ before reduction (kg) and $m_{ra}$ is the mass of $Fe_3O_4$ after reduction (kg).

Flotation experiment. To investigate the effect of the $FeS_2$-C reductant pellet ($FeS_2$:C = 7:3) on the recovery of copper in the slag, the flotation results of CS without a reductant were compared with that after being reduced by the $FeS_2$-C reductant pellet ($FeS_2$:C = 7:3). The CS powder was provided by smashing it with a hammer and grinding in a ball mill after solidifying in the furnace during the dilution experiment, which contained 80% powder particles with a size of – 74 $\mu$m. All the CS powder was weighed ($m_1$) first and then, after a series of steps of flotation, filtration, drying, and weighing, the slag powder could be separated into concentrate ($m_2$) and tailings ($m_3$). Finally, the dried samples of the concentrate and tailings were analyzed, and the copper content in the concentrate was $\beta$ and the

copper content in the tailings was $\theta$. In the flotation process, some reagents should be added for effectively recovering the copper in the slag. Lime (CaO) is a common regulator and inhibitor in the separation of copper sulfide and pyrite that can adjust the pH value of the pulp of CS to 9–11 and inhibit pyrite for promoting copper recovery.[38] Zinc sulfate ($ZnSO_4$) is a common and good inhibitor to recover copper from copper mineral with zinc, so that $Zn^{2+}$ from $ZnSO_4$ forms complexes under alkaline conditions, adhering to the surface of the zinc mineral (in CS), covering the active site of its interaction with the collector.[10] O-isopropyl ethylthiocarbamate (Z-200, $C_6H_{13}NOS$) is a collector for the flotation of copper sulfide mineral, while CS is a kind of synthetic copper sulfide mineral that can collect exposed copper in the pulp of CS for easily recovering the copper.[10] Terpenic oil ($2^{\#}$ oil, $C_{10}H_{18}O$) is an excellent frother for copper in the flotation process that can form stable foam for carrying the collector with the copper. The process parameters are shown in Table III.

Copper recovery in concentrate:

$$\gamma = \frac{\beta m_2}{\alpha m_1} \times 100\%. \quad (4)$$

Ratio of copper content in tailings:

$$\gamma = \frac{\theta m_3}{\alpha m_1} \times 100\% \quad (5)$$

where $\alpha$ is the copper content in the CS before flotation.

### Characterization

The slag composition was determined by the inductively coupled plasma–optical emission spectrometry (iCAP 7200; Thermo Fisher Scientific, USA) and chemical titration (GB/T 6730.65-2009). The micromorphology and element distribution were detected by scanning electron microscope–energy-dispersive spectroscopy (SEM-EDS; Pure, USA). The Cu content was obtained by an atomic absorption spectrometer (AA-6880; Shimadzu, Japan). The density of the samples, including reductant, slag, and matte, was measured by a true density analyzer (AccuPyc II 1340 V1.05, Micromeritics, USA). The $Fe_3O_4$ content was determined by the method of chemical titration after magnetic separation. The content of magnetic iron, including $Fe_3O_4$ and metal Fe, was obtained by magnetic separation, in which metal Fe might be generated by adding excessive reductant from the high-temperature reduction test in this paper. The content of metal Fe in the slag was measured by the cupric potassium chloride method with standard potassium permanganate titrating.[39–41] The $Fe_3O_4$ content in the slag was calculated on the basis of the metal Fe content and the magnetic iron content.

The reaction Gibbs free energy and the equilibrium composition analysis of $Fe_3O_4$ in the CS with reductant were calculated by the software of HSC Chemistry 6, which were obtained by the Reaction Equations module and the Equilibrium Compositions module, respectively.

The reductant pellet and the copper matte droplets settling in the molten slag were simulated by finite element analysis. The parameters in the calculation and simulation are shown in Table IV

The models for the simulation are displayed in Fig. 3 with the building parameters shown in Table V and the mesh parameters shown in Table VI.

**Table III. The parameters of the flotation process**

| Remarks | Parameter |
|---|---|
| Grinding time | 1 min |
| Mass of CS for flotation | 300 g |
| Dosage of CaO | 1000 g/t |
| Dosage of $ZnSO_4$ | 3000 g/t |
| Dosage of Z-200 | 120 g/t |
| Dosage of $2^{\#}$oil | 2 drops |
| Flotation temperature | 25°C |

## RESULTS AND DISCUSSION

### Challenges and Solution for Low-Density and Powdery Reductants

The low density of the reductant is one challenge that limits the reduction kinetics of $Fe_3O_4$ by coal. The increase of $Fe_3O_4$ content in molten CS will lead to precipitation of more solid $Fe_3O_4$ particles, resulting in a great increase of the slag viscosity (Fig. 4a).[12] The increased slag viscosity in turn restrains the settling of the entrained copper matte droplets in the molten slag (Fig. 4b), hindering the copper–slag separation during the molten-stage process.[19] Also, the precipitated $Fe_3O_4$ particles with high hardness tend to tightly wrap the copper matte droplets (Fig. 4c), which leads to increased difficulty for copper exposure during grinding in the cold-state process for copper recovery.[43] Elimination of $Fe_3O_4$ particles using coal as the reductant has been adopted because of its strong reduction ability; however, it is retarded by its unfavorable reaction kinetics. Specifically, the coal generally floats on the upper surface of molten CS due to its much lower density than the molten slag (1.75 g/cm$^3$ vs. 3.70 g/cm$^3$), which is evidenced by the coal pellet floating after dropping it into the molten slag (Fig. 4d). Such a floating state leads to barely any reduction of $Fe_3O_4$ on the lower parts of the slag, as shown by the negligible change of $Fe_3O_4$ content in site 2 (17.10% $Fe_3O_4$; Fig. 4d) compared with that of the original CS (18.80% $Fe_3O_4$; Fig. 4d). The floating state of the anthracite pellet is also manifested by the finite element analytical result (Fig. 4e) where the white block is an anthracite pellet and the color

**Table IV. The physical property parameters used in the simulations**

| Parameter | Value | Unite | Remarks |
|---|---|---|---|
| $\rho_{FeS_2-C}$ | 4.02 | g/cm$^3$ | Density of $FeS_2$-C reductant pellet ($FeS_2$:C = 7:3) |
| $\rho_C$ | 1.75 | g/cm$^3$ | Density of C reductant pellet |
| $\rho_{CS}$ | 3.7 | g/cm$^3$ | Density of CS |
| $\rho_{matte}$ | 5.2 | g/cm$^3$ | Density of matte |
| $\mu_{CS}$ | 0.1, 0.25, 0.7 | Pa s | Viscosity of CS |
| $\mu_{matte}$ | $\mu_{CS} \times 0.015$[a] | – | Viscosity of matte |
| $\sigma$ | 0.58 | N/m | Surface tension of slag[42] |

[a]0.015 is the median value of 1/50–1/100 which is the ratio of the viscosity of matte to the viscosity of CS.[15]

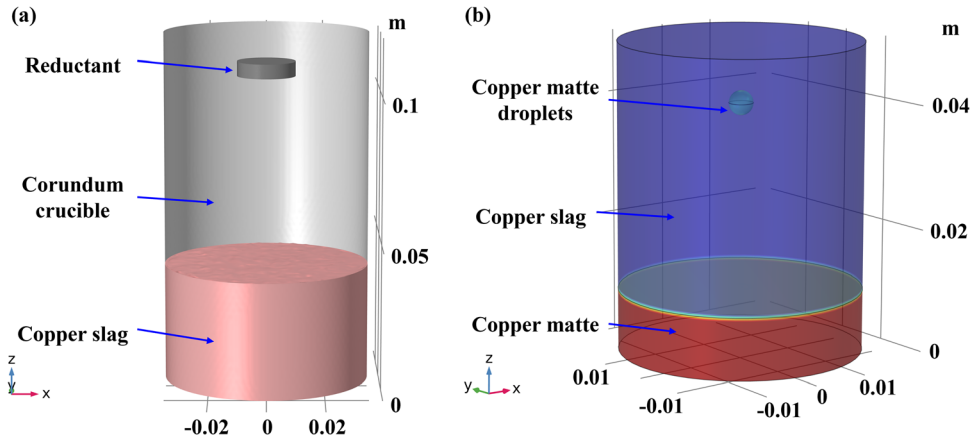


Fig. 3. The simulation model of (a) the reductant pellet settling in the melting slag, (b) the copper matte droplet settling in the melting slag.

**Table V. The building parameters of the models**

| Parameter | Value | Unite | Remarks |
|---|---|---|---|
| *Model of reductant pellet settling* | | | |
| $H_{CS}$ | 0.04 | m | Height of molten slag |
| $D_c$ | 0.06 | m | Diameter of crucible |
| $D_r$ | 0.02 | m | Diameter of reductant pellet |
| $h_r$ | 0.005 | m | Height of reductant pellet |
| $H_r$ | 0.1 | m | Initial height of reductant pellet |
| $v_i$ | 4.2 | m/s | Initial velocity of reductant pellet |
| $g$ | 9.8 | m/s$^2$ | Acceleration of gravity |
| *Model of copper matte droplets settling* | | | |
| $H_{melt}$ | 0.05 | m | Height of melt |
| $H_{matte}$ | 0.01 | m | Height of copper matte |
| $d_{matte}$ | 0.002 | m | Copper matte droplets size |
| $h_{matte}$ | 0.04 | m | Height of matte droplets |

region represents the molten CS (the darker the red, the higher the speed of molten CS, whereas the darker the blue, the lower the speed of molten CS), that means that the coal pellet still floats on the surface after adding it into the molten CS for 10 min. Therefore, coal with very low density will float and accumulate on the surface of the molten slag, which provides a very limited coal–slag contact surface area (Fig. 4f), challenging the high-efficiency elimination of the $Fe_3O_4$ particles.

In addition to the low density, the low reduction ability of the reductant in the powdery state is another challenge for high-efficiency reduction of $Fe_3O_4$.[37,44,45] Compared with the coal with low

**Table VI. The mesh parameter of the models**

| Model of reductant pellet settling | | Model of copper matte droplets settling | |
|---|---|---|---|
| **Parameter** | **Remarks** | **Parameter** | **Remarks** |
| 5997 | Mesh vertices | 4338 | Mesh vertices |
| 9606 | Triangles | 8421 | Triangles |
| 1072 | Quads | None | Quads |
| 316 | Edge elements | 303 | Edge elements |
| 8 | Vertex elements | 10 | Vertex elements |
| 10678 | Number of elements | 8421 | Number of elements |
| 0.1046 | Minimum element quality | 0.5774 | Minimum element quality |
| 0.8478 | Average element quality | 0.9409 | Average element quality |

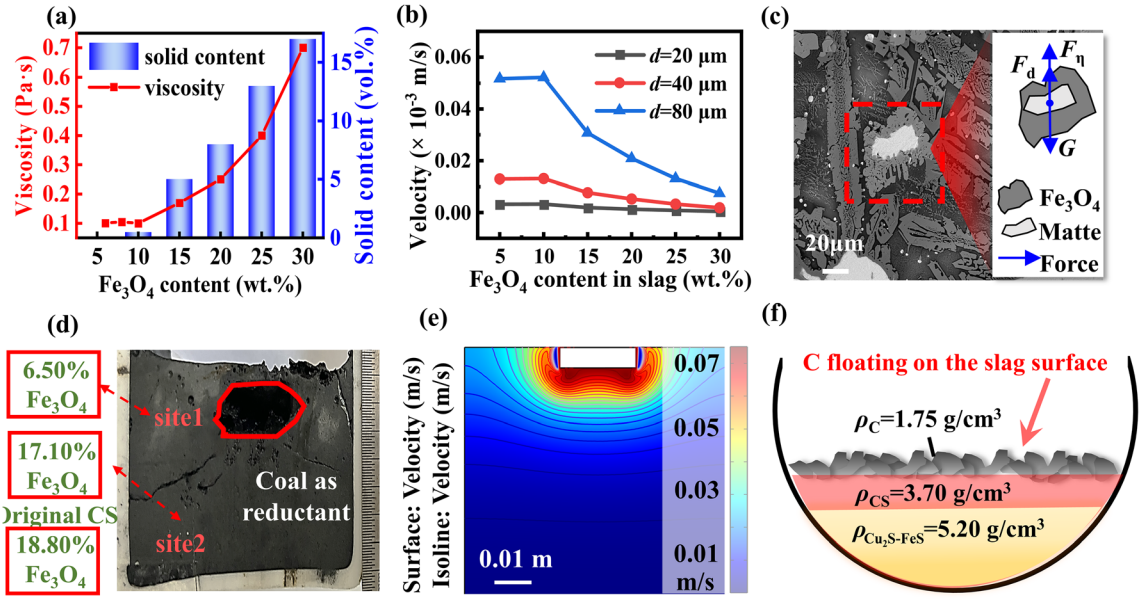


Fig. 4. (a) Effect of $Fe_3O_4$ content on viscosity and solid content in molten CS (denoted as reference 12); (b) effect of $Fe_3O_4$ content in molten slag on the velocity of matte droplet (calculated by Eq. 2); (c) SEM images for one typical $Fe_3O_4$-wrapping copper matte microstructure and the corresponding illustration in the *inset* ($F_d$ drag force, $F_\eta$ viscos drag, $G$ gravity); (d) cross-section of the solidified slag using a coal pellet as the reductant; the original CS is the untreated copper slag; (e) simulated final site of the pellet ($\rho$ = 1.75 g/cm$^3$, equal to the density of coal) after settling in the molten slag ($\rho$ = 3.7 g/cm$^3$) for 10 min; (f) the powdery carbon floating on the surface of the molten CS.

density ($\rho$ = 1.75 g/cm$^3$), the $FeS_2$ possesses a much higher density ($\rho$ = 4.99 g/cm$^3$), which means that floatation of reductants on the upper surface of molten slag can be hopefully avoided. However, only a slight decrease of the $Fe_3O_4$ content, from 17.1% to 14.9% (Fig. 5a) is observed in the lower layer of the solidified slag after replacing the low-density coal with high-density $FeS_2$ as the reductant, which means that the high-density powdery $FeS_2$ is not efficiently sunk into the molten slag to take part in the reaction. This contradiction is possibly due to the large repelling force induced by the interfacial tension for powdery reductants.[19,44] Another reason for the insufficient reduction of $Fe_3O_4$ is due to the much lower reduction ability of $FeS_2$ than that of coal, as manifested by the comparison of the Gibbs free energy changes of related reactions (Fig. 5b).[19] It should be noted that the powdery reductants can be easily blown away by the high-pressure off-gas in a real industrial atmosphere, further decreasing the reaction ability of powdery reductants.

The challenges of low density and powdery state as well as insufficient reduction ability can be resolved by density tuning in conjunction with pelletizing of the powdery mixture of coal and $FeS_2$. As shown in Fig. 5c, mixing the 70% $FeS_2$ and 30% coal powders can turn the density from 1.75 g/cm$^3$ (pure coal) to 4.02 g/cm$^3$ (slag density: 3.70 g/cm$^3$).[15] After die-pressing into pellets, the as-prepared composite reductant can efficiently sink into the molten slag (Fig. 5c), which is in high agreement with the simulation result by finite element analysis (Fig. 5d). The pellets will not deform after dropping into the molten slag. To prove that, the pellet was heated to the experiment temperature of 1250°C and kept for 60 min in Ar

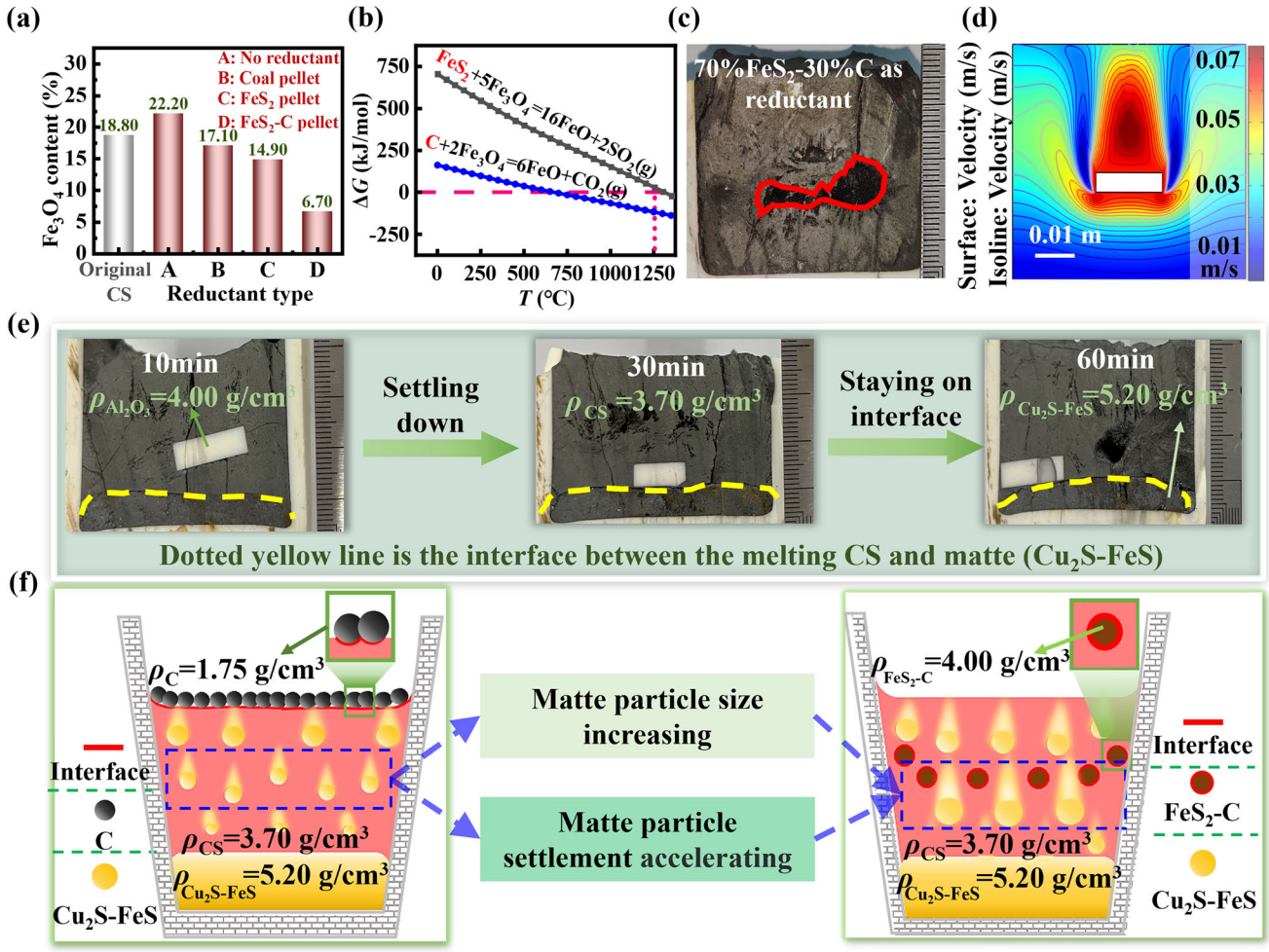


Fig. 5. (a) Effects of reductant type (*A* no-reductant, *B* coal pellet, *C* $FeS_2$ pellet, *D* $FeS_2$-C pellet ($FeS_2$:C = 7:3)) on $Fe_3O_4$ content in the lower layer of the slag; (b) reaction Gibbs free energy for coal and $FeS_2$; (c) cross-sectional images of the solidified CS after dropping the $FeS_2$-C composite pellet ($FeS_2$:C = 7:3); (d) simulated final site of the pellet ($\rho$ = 4.02 g/cm$^3$, equal to the $FeS_2$-C pellet with mass ratio of 7:3) after settling in molten slag ($\rho$ = 3.70 g/cm$^3$) for 10 min; (e) settling of the reaction-inert corundum pellet with the density between copper matte and slag; (f) the reduction by powdery coal and $FeS_2$-C composite pellets.

gas atmosphere. Consequently. the pellet still kept contact after keeping at the high temperature for such a long period, meaning that the pellet can remain undeformed in the molten bath before disappearance by chemical reaction. The avoided floatation of the $FeS_2$-C pellet is also verified by the time-dependent sinking behavior of the reaction-inert corundum pellet, which possesses the same density and size as the $FeS_2$-C pellet (Fig. 5e). Also, such a mixing strategy between coal and $FeS_2$ can provide a higher reduction ability than single $FeS_2$, thus mitigating the challenge of insufficient reduction ability.[43] Moreover, the addition of coal can also decrease the pellet-forming difficulty for powdery $FeS_2$. Resultantly, the $Fe_3O_4$ content in the lower layer is significantly decreased from 17.10% for coal pellet and 14.90% for $FeS_2$ powder to 6.70% for the $FeS_2$-C pellet.

In a word, the density tuning in conjunction with pelletizing of the powdery $FeS_2$ and coal contribute to more efficient sink and stronger reduction ability of the composite reductants. Resultantly, the elimination of the $Fe_3O_4$ particles is much enhanced as shown in Fig. 5f.

## Enhanced Copper Matter Settling for Copper-Slag Separation in Molten State

Turning the powdery coal into $FeS_2$-C pellets can enhance the $Fe_3O_4$ elimination efficiency, which can lower the slag viscosity, promoting the settling of matte droplets for more efficient copper–slag separation. As shown in Fig. 6a, the density of the pellet can be tuned by changing the added amount of $FeS_2$, which can be located in the range of 1.75–4.99 g/cm$^3$. Using the pellets with different densities as the reductants, the variation of copper content in different parts of the solidified slag (Fig. 6b) is understood, showing that 70% $FeS_2$ in the pellet is the best option, contributing to the highest copper content in the lower layer (4.53% Cu; Fig. 6b1), the lowest copper content in the middle layer (0.48% Cu;

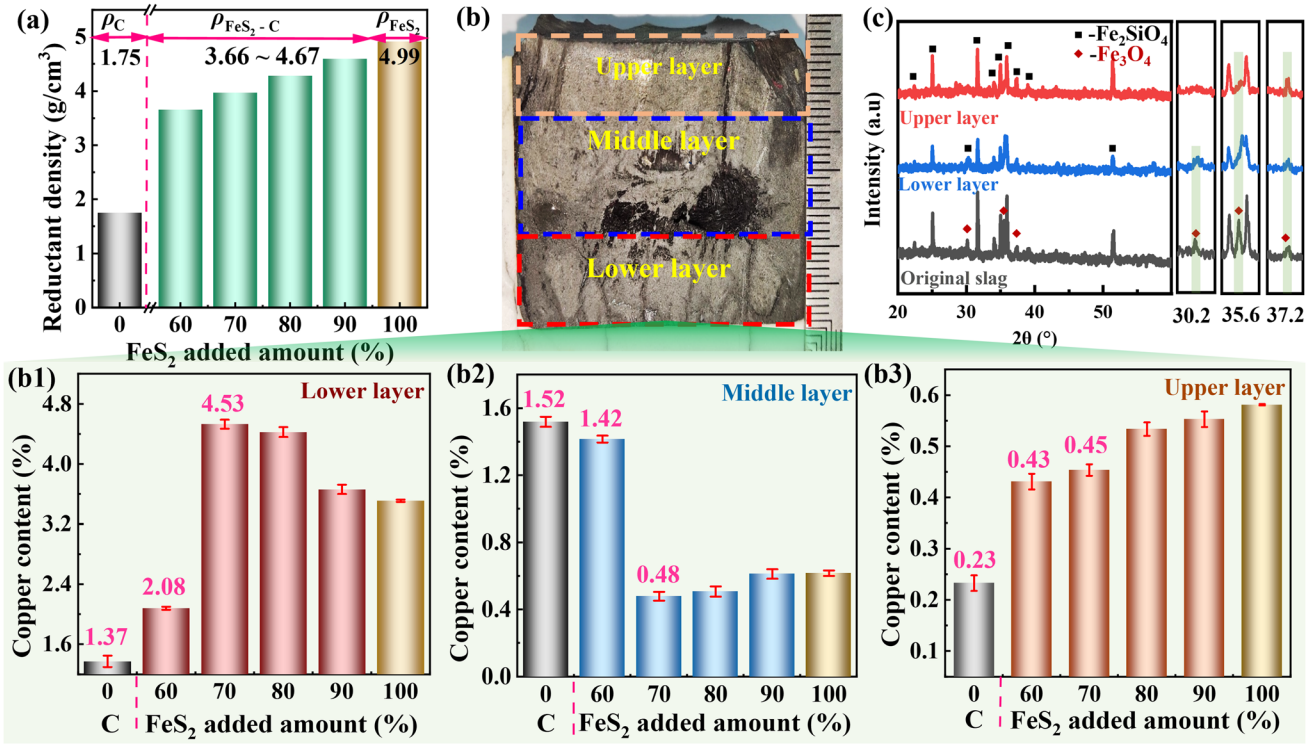


Fig. 6. (a) Reductant density with adding different amounts of $FeS_2$; (b) cross-section of one typical solidified CS, wherein the copper content of (b1) the upper layer, (b2) middle layer, and (b3) lower layer are analyzed; (c) XRD pattern of reduced slag compared with the original CS.

Fig. 6b2), and very low copper content in the upper layer (0.45% Cu; Fig. 6b3). All the cases for $FeS_2$-C pellets show more appealing results than those of both pure coal and 100% $FeS_2$ (Fig. 6b1, b2 and b3). The XRD patterns of reduced slag also indicated that the elimination of $Fe_3O_4$ were achieved by the $FeS_2$-C pellet (Fig. 6c). For the optimized pellet composition containing 70%$FeS_2$, the reduction efficiency of $Fe_3O_4$ can be increased from 18% to 51%, as calculated by Eq. 3. These results mean that the composition optimization of the pellet can facilitate the settling of copper matte droplets, contributing to much enhanced copper–slag separation during the hot-stage process.

The enhanced settling of the copper matte droplets is attributed to the $Fe_3O_4$-elimination-induced viscosity decrease and the $Fe_3O_4$ reduction-induced matte droplet coalescence. As shown in Fig. 7a, elimination of $Fe_3O_4$ can result in the obvious decrease of the slag viscosity,[9,31] which facilitates the settling of the copper matte droplets,[19,46] as shown by the inset simulation results. Specifically, the settling distance of the matte droplet is only 20% of the total slag height (denoted as h in Fig. 7a) for the slag with 0.7 Pa s, which is increased to 60% for slag with 0.25 Pa s and totally enters into the bottom copper matte layer for slag with 0.1 Pa s. The enhanced elimination of $Fe_3O_4$ after replacing the $FeS_2$ with $FeS_2$-C is due to the stronger reduction ability for the latter case, as shown by the comparison of the final equilibrium composition for these two cases (Fig. 7b, c), being consistent with the result in Fig. 5b. The lower content of $Fe_3O_4$ particles in the molten slag facilitates the exposure of the copper matte droplets and subsequently their coalescence.[43] This enhanced coalescence is manifested by the morphology observations of the slags after reduction by different cases (bright area denotes copper matte in Fig. 7d, e, and f), which show that the size of the typical copper matte droplet in $FeS_2$-C ($\sim$ 100 $\mu$m) is much higher than both the reductant-free case ($\sim$ 10 $\mu$m) and pure $FeS_2$ ($\sim$ 50 $\mu$m). Also, the exposure and coalescence of the matte droplets can be understood by the composition analysis of microregions in the SEM results (Fig. 7g, h and i), showing that the $Fe_3O_4$-wrapping copper matte droplets with small size in the original slag (Fig. 7d, g, blue particles: $Fe_3O_4$) are turned to isolated copper matte droplets with much larger sizes (Fig. 7e, h). Compared to the pure $FeS_2$ (Fig. 7f, i), the $FeS_2$-C pellet (Fig. 7e, h) presents much deeper breaking of the $Fe_3O_4$-wrapping copper matte structure.

Therefore, turning the powdery coal into $FeS_2$-C pellets can enhance the $Fe_3O_4$ elimination efficiency, which can lower the slag viscosity and as a result promote the settling of matte droplets for more efficient copper–slag separation in the molten state. Also, the enhanced settling of the matte

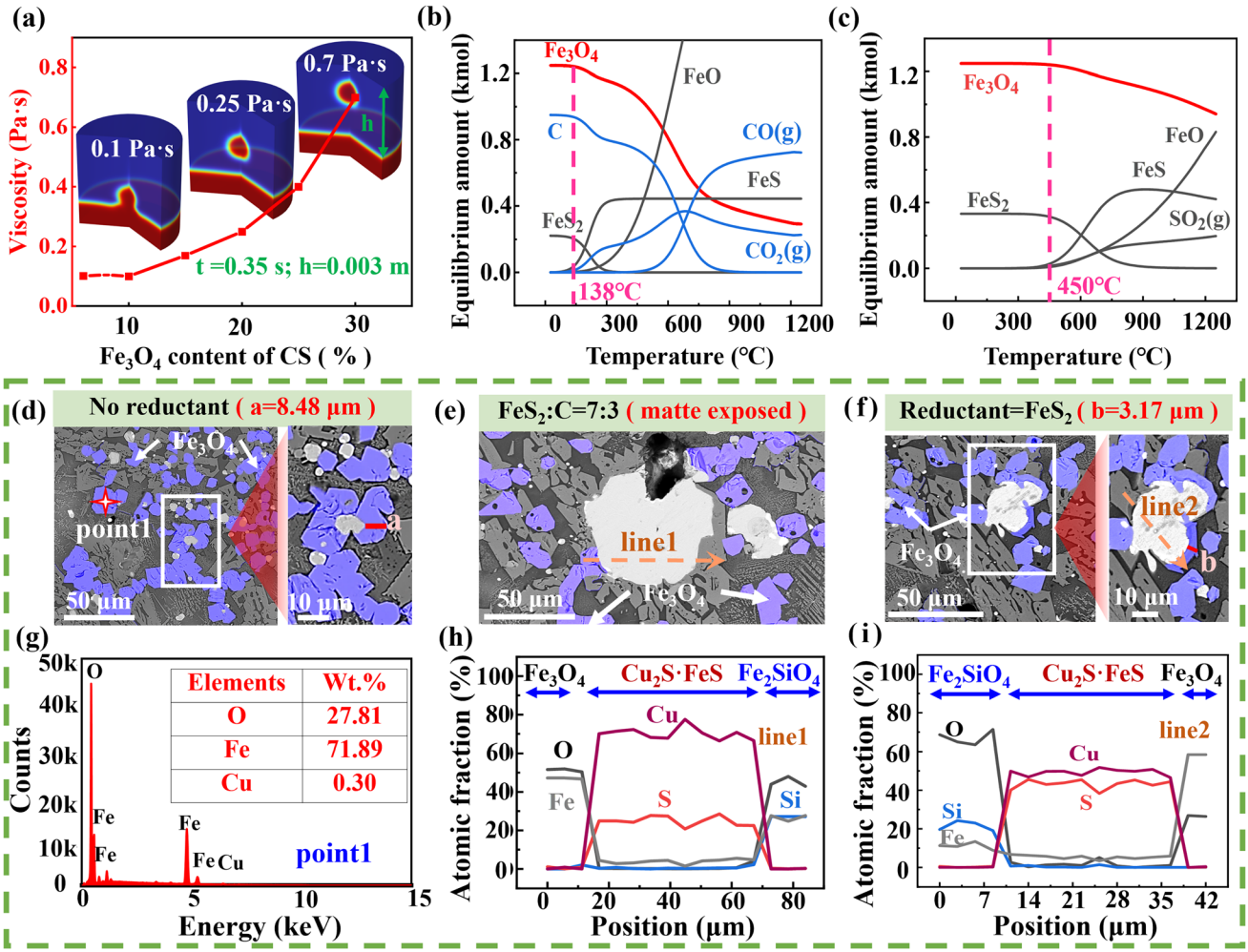


Fig. 7. (a) Relationship between the slag viscosity and $Fe_3O_4$ content as well as the settling behavior of the matte droplet; the equilibrium composition of the CS after reduction by the $FeS_2$-C pellet ($FeS_2$:C = 7:3) (b) and pure $FeS_2$ (c). For (b), the initial components are 1.25 kmol $Fe_3O_4$, 0.22 kmol $FeS_2$, and 0.95 kmol C. For (c), the initial components are 1.25 kmol $Fe_3O_4$, 0.33 kmol $FeS_2$, which were the same quality of CS and reductant as (b). SEM images and the EDS results of the solidified slags in the lower layer after reduction by no reductant (d, g), $FeS_2$-C (e, h), and $FeS_2$ (f, i). *Blue particles* denote $Fe_3O_4$, the *bright particles* point to the copper matte, and the *light gray areas* are $Fe_2SiO_4$. (g)–(i) are the results for *point 1* in (d), *line 1* in (e), and *line 2* in (f), respectively (Color figure online).

droplets is attributed to the full exposure of the $Fe_3O_4$-wrapped copper matte droplets and its subsequent droplet–droplet coalescence for size growth. The enhanced settling of copper matte droplets can promise preliminary enrichment in the molten state while the copper exposure and size growth of the copper matte can hopefully facilitate the further enrichment of copper during the subsequent grinding–floatation process for the solidified cold slag.

## Further Copper Enrichment During Floatation of Solidified Cold Slag

The typical process for copper smelter plants is presented in Fig. 8. Generally, $FeS_2$ concentrate is generated after flotation of primary copper ore while the smelting slag containing ~ 1% Cu is produced from the copper concentrate after the smelting furnace (Fig. 8a). Preliminary enrichment of copper in the smelting slag in industry is realized by standing the molten slag for a period of time with the aid of adding reductants, with this process also being called dilution (Fig. 8a). The remaining copper in the diluted slag is further recovered as copper concentrate by the grinding–flotation process.

Here, by replacing the industrial coal or $FeS_2$ powders with the $FeS_2$-C pellets as the reductants for dilution (Fig. 8a), both the exposure and the size growth of the copper matte droplets in the molten slag are greatly promoted, which can enhance the subsequent copper recovery from the solidified slag by the grinding–flotation process. As shown in Fig. 8b, the same grinding–flotation process has been adopted for the cases of the original slag without adding reductant, pure coal, and pure $FeS_2$, as well as the $FeS_2$-C composite pellet, resulting in copper concentrate and tailings. Obviously, the $FeS_2$-C pellet case shows the highest copper recovery of 85.3% after only a one-step preliminary flotation, with the concentrate grade also being the

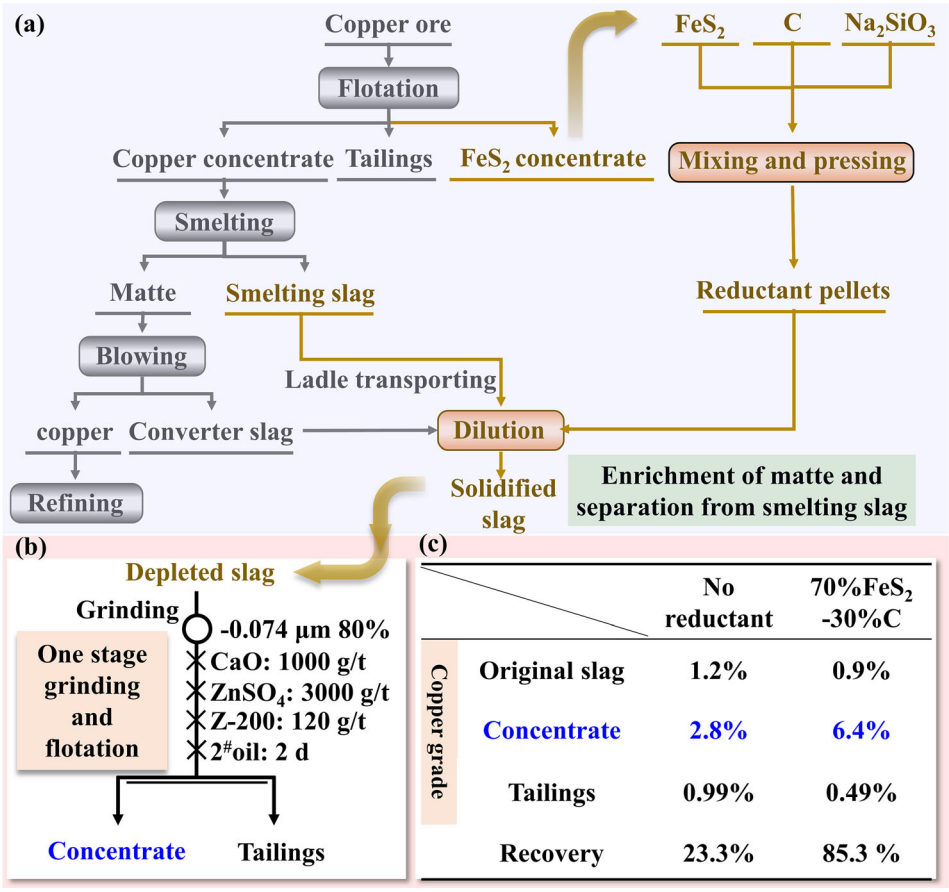


Fig. 8. The copper recovery of copper using $FeS_2$-C: (a) $FeS_2$ self-circulating in the copper smelting process; (b) flotation process of CS after reduction; (c) flotation results.

highest (6.4%). The results strongly prove that the as-prepared $FeS_2$-C pellet can not only promote the settling of copper matte droplets for copper–slag separation in molten state but also enhance the further copper recovery from the solidified slag in the cold grinding–flotation stage.

## CONCLUSIONS

A new strategy for designing high-activity reductants to improve the copper recovery ratio has been realized. By replacing the industry-used powdery coal with the $FeS_2$-C pellets as the reductant, the elimination efficiency of $Fe_3O_4$ particles in the molten slag is greatly increased from 15% to 51%, resulting in a great decrease of the slag viscosity and enhanced settling of the copper matte droplets. Also, the promoted reduction of $Fe_3O_4$ facilitates the full exposure of the $Fe_3O_4$-wrapped copper matte droplets and their subsequent size growth by coalescence, conjointly promoting the settling behavior of the droplets. The $FeS_2$-C pellet with the optimized composition contains 70% $FeS_2$, which shows a density of 4 g/cm$^3$, with the copper content in the low-layer slag being enriched from 1.37% to 4.53%. Additionally, the full exposure and size growth of the copper matte is also beneficial to the copper recovery during the subsequent grinding–flotation process of the solidified slag, which increases the copper recovery from 23.3% to 85.3% after only one-stage flotation, with the concentrate grade being correspondingly improved from 2.8% to 6.45%. These results can provide new insights into enhancing the recovery of the slag-entrained copper.

## ACKNOWLEDGMENTS

This research was funded by the National Key Basic Research and Development Program (No. 2023YFC2907903), National Natural Science Foundation (No. 52274349), Fujian Province Natural Science Foundation (No. 2023J05024), and Fujian Province University-Industry Cooperation Research Program (No. 2023H6007).

## CONFLICT OF INTEREST

The authors declare that they have no conflict of interest.

## REFERENCES


1. T. Kundu, S. Senapati, S.K. Das, S.I. Angadi, and S.S. Rath, *Powder Technol.* 426, 118693 https://doi.org/10.1016/j.powtec.2023.118693 (2023).
2. W.P. Liu and X.F. Yin, *Int. J. Miner. Metall. Mater.* 24, 621 https://doi.org/10.1007/s12613-017-1444-z (2017).
3. R. Sharma and R.A. Khan, *J. Clean. Prod.* 151, 179 https://doi.org/10.1016/j.jclepro.2017.03.031 (2017).
4. A. Rusen, B. Derin, A. Geveci, and Y.A. Topkaya, *JOM* 68, 2316 https://doi.org/10.1007/s11837-016-1954-6 (2016).
5. K. Mikula, G. Izydorczyk, D. Skrzypczak, K. Moustakas, A. Witek-Krowiak, and K. Chojnacka, *J. Hazard. Mater.* 403, 123602 https://doi.org/10.1016/j.jhazmat.2020.123602 (2021).
6. Z.W. Zhao, Z.B. Wang, W.B. Xu, W.N. Qin, J. Lei, Z.Q. Dong, and Y.J. Liang, *J. Hazard. Mater.* 415, 125642 https://doi.org/10.1016/j.jhazmat.2021.125642 (2021).
7. Q.M. Wang, S.S. Wang, M. Tian, D.X. Tang, Q.H. Tian, and X.Y. Guo, *Int. J. Miner. Metall. Mater.* 26, 301 https://doi.org/10.1007/s12613-019-1738-4 (2019).
8. M.A. Topçu, A. Rüşen, and B. Derin, *J. Mater. Res. Technol.* 8, 6244 https://doi.org/10.1016/j.jmrt.2019.10.018 (2019).
9. H.P. Zhang, B. Li, Y.G. Wei, H. Wang, Y.D. Yang, and A. Mclean, *Metall. Mater. Trans. B* 51, 2663 https://doi.org/10.1007/s11663-020-01963-0 (2020).
10. X.P. Chi, Z.H. Ye, H. Wang, W. Weng, and S.P. Zhong, *Miner. Eng.* 202, 108275 https://doi.org/10.1016/j.mineng.2023.108275 (2023).
11. J.L. Zhang, X. Yang, J.K. Zhang, Y.Q. Chen, L.F. Zhang, and C.Y. Wang, *Chin. J. Nonferrous Met.* 29, 1712 https://doi.org/10.19476/j.ysxb.1004.0609.2019.08.16 (2019).
12. L. Sheng, J.T. Li, J.K. Zhang, J.L. Zhang, L.F. Zhang, and X.M. Hou, *Chin. J. Eng.* 39, 48 https://doi.org/10.13374/j.issn2095-9389.2017.01.006 (2017).
13. R.L. Zheng, J.F. Lv, W.F. Song, M.D. Liu, H. Li, Y. Liu, X.J. Lv, and Z.Y. Ma, *Int. J. Miner. Metall. Mater.* 30, 886 https://doi.org/10.1007/s12613-022-2569-2 (2023).
14. S.W. Zhou, Y.G. Wei, B. Li, and H. Wang, *J. Clean. Prod.* 217, 423 https://doi.org/10.1016/j.jclepro.2019.01.184 (2019).
15. R.L. Zheng, J.F. Lv, W.F. Song, M.D. Liu, H.S. Li, Y. Liu, X.J. Lv, and Z.Y. Ma, *Int. J. Miner. Metall. Mater.* 30, 886 https://doi.org/10.1007/s12613-022-2569-2 (2023).
16. Z.L. Zuo, Q.B. Yu, H.Q. Xie, F. Yang, Z.C. Han, and Q. Qin, *Environ. Technol.* 41, 2240 https://doi.org/10.1080/09593330.2018.1561757 (2020).
17. K.Q. Li, S. Ping, H.Y. Wang, and W. Ni, *Int. J. Miner. Metall. Mater.* 20, 1035 https://doi.org/10.1007/s12613-013-0831-3 (2013).
18. P. Taskinen and A. Jokilaakso, *Metall. Mater. Trans. B* 52, 3524 https://doi.org/10.1007/s11663-021-02283-7 (2021).
19. K. Wang, Y. Liu, J. Hao, Z.H. Dou, G.Z. Lv, and T.A. Zhang, *Trans. Nonferrous Met. Soc. China* 33, 2511 https://doi.org/10.1016/S1003-6326(23)66277-6 (2023).
20. A. Warczok and T.A. Utigard, *Can. Metall. Q.* 37, 27 https://doi.org/10.1016/S0008-4433(97)00034-7 (1998).
21. L.F. Zhang, S.Q. Wang, A.P. Dong, J.W. Gao, and L.N.W. Damoah, *Metall. Mater. Trans. B* 45, 2153 https://doi.org/10.1007/s11663-014-0123-y (2014).
22. B.J. Zhang, T.A. Zhang, Z.H. Dou, and D.L. Zhang, *J. Wuhan Univ. Technol. Mater. Sci. Ed.* 37, 699 https://doi.org/10.1007/s11595-022-2584-1 (2022).
23. B.J. Zhang, L.P. Niu, T.A. Zhang, Z.Q. Li, D.L. Zhang, and C. Zheng, *ISIJ Int.* 57, 775 https://doi.org/10.2355/isijinternational.ISIJINT-2016-631 (2017).
24. Z.W. Wang, J.T. Gao, X. Lan, and Z.C. Guo, *J. Hazard. Mater.* 468, 133834 https://doi.org/10.1016/j.jhazmat.2024.133834 (2024).
25. X. Lan, J.T. Gao, Z.L. Huang, and Z.C. Guo, *Metall. Mater. Trans. B* 49, 1165 https://doi.org/10.1007/s11663-018-1235-6 (2018).
26. Z.W. Wang, J.T. Gao, X. Lan, G.L. Feng, and Z.C. Guo, *Resour. Conserv. Recycl.* 182, 106316 https://doi.org/10.1016/j.resconrec.2022.106316 (2022).
27. X.C. Wen, L. Guo, Q.P. Bao, and Z.C. Guo, *Int. J. Miner. Metall. Mater.* 28, 1929 https://doi.org/10.1007/s12613-020-2118-9 (2021).
28. M. Kalisch, B. Friedrich, and M.A. Reuter, *Metall. Mater. Trans. B* 54, 1017 https://doi.org/10.1007/s11663-023-02758-9 (2023).
29. J.L. Du, F.X. Zhang, J.H. Hu, S.L. Yang, H.L. Liu, and H. Wang, *J. Clean. Prod.* 363, 132546 https://doi.org/10.1016/j.jclepro.2022.132546 (2022).
30. B. Li, Y.G. Wei, H. Wang, and Y.D. Yang, *ISIJ Int.* 58, 1168 https://doi.org/10.2355/isijinternational.ISIJINT-2017-723 (2018).
31. H.P. Zhang, B. Li, Y.G. Wei, and H. Wang, *J. Mater. Res. Technol.* 15, 6216 https://doi.org/10.1016/j.jmrt.2021.11.061 (2021).
32. H.P. Zhang, B. Li, A. McLean, Y.G. Wei, H. Wang, and Z.L. Ye, *Metall. Mater. Trans. B* 54, 178 https://doi.org/10.1007/s11663-022-02678-0 (2023).
33. H.D. Dong, Y.G. Wei, S.W. Zhou, B. Li, and H. Wang, *Sustain. Chem. Pharm.* 22, 100482 https://doi.org/10.1016/j.scp.2021.100482 (2021).
34. Y.G. Wei, T.F. Zhang, B. Li, and S.W. Zhou, *Metall. Mater. Trans. B* 51, 2756 https://doi.org/10.1007/s11663-020-01986-7 (2020).
35. K. Maweja, T. Mukongo, and I. Mutombo, *J. Hazard. Mater.* 164, 856 https://doi.org/10.1016/j.jhazmat.2008.08.107 (2009).
36. X.B. Wan, P. Taskinen, J.J. Shi, and A. Jokilaakso, *J. Hazard. Mater.* 414, 125541 https://doi.org/10.1016/j.jhazmat.2021.125541 (2021).
37. X. Yang, J.L. Zhang, J.K. Zhang, J.H. Hu, J.T. Li, L.F. Zhang, Y.Q. Chen, and C.Y. Wang, *Metall. Mater. Trans. B* 49, 3118 https://doi.org/10.1007/s11663-018-1396-3 (2018).
38. Q.C. Feng, W.H. Yang, M.H. Chang, S.M. Wen, D.W. Liu, and G. Han, *Int. J. Miner. Metall. Mater.* 31, 1 https://doi.org/10.1007/s12613-023-2709-3 (2024).
39. J. Riott, *Anal. Chem.* 13, 546 https://doi.org/10.1021/i560096a011 (1941).
40. J. Byars and T.W. McCreary, *J. Chem. Educ.* 69, 935 https://doi.org/10.1021/ed069p935 (1992).
41. M.G. Habashy, *Anal. Chem.* 33, 586 https://doi.org/10.1021/ac60172a032 (1961).
42. H.W. Zhang, L. Fu, J.B. Qi, and W.D. Xuan, *Metall. Mater. Trans. B* 50, 1852 https://doi.org/10.1007/s11663-019-01611-2 (2019).
43. S.W. Zhou, Y.G. Wei, Y. Shi, B. Li, and H. Wang, *Metall. Mater. Trans. B* 49, 2458 https://doi.org/10.1007/s11663-018-1364-y (2018).
44. N. Dosmukhamedov, M. Egizekov, E. Zholdasbay, and V. Kaplan, *JOM* 70, 2400 https://doi.org/10.1007/s11837-018-3093-8 (2018).
45. B.J. Zhang, T.A. Zhang, L.P. Niu, N.S. Liu, Z.H. Dou, and Z.Q. Li, *JOM* 70, 47 https://doi.org/10.1007/s11837-017-2670-6 (2018).
46. Y.X. Liu, Y.G. Wei, S.W. Zhou, B. Li, and H. Wang, *J. Min. Metall. Sect. B Metall.* 59, 27 https://doi.org/10.2298/JMMB220421003L (2023).